Metal-like Charge Transport in PEDOT(OH) Films by Post-processing Side Chain Removal from a Soluble Precursor Polymer

James F. Ponder Jr.,[a,b]* *Shawn A. Gregory,*[c] *Amalie Atassi,*[c] *Abigail A. Advincula,*[c] *Joshua M. Rinehart,*[c] *Guillaume Freychet,*[d] *Gregory M. Su,*[e] *Shannon K. Yee,*[a] *and John R. Reynolds*[c,f]

a George W. Woodruff School of Mechanical Engineering, Georgia Institute of Technology, Atlanta, GA 30332, USA.

b Materials and Manufacturing Directorate, Air Force Research Laboratory, Wright-Patterson AFB, Ohio 45433, United States; UES, Inc., Dayton, Ohio 45432, United States (current address)

c School of Materials Science and Engineering, Georgia Institute of Technology, Atlanta, GA 30332, USA.

d NSLS-II, Brookhaven National Laboratory, Upton, New York, 11973, United States

e Advanced Light Source & Materials Sciences Division, Lawrence Berkeley National Laboratory, Berkeley, California, 94720, United States

f School of Chemistry and Biochemistry, Center for Organic Photonics and Electronics, Georgia Tech Polymer Network, Georgia Institute of Technology, Atlanta, GA 30332, USA.

Corresponding Author *E-mail: jponder7@gatech.edu

Keywords: Post-polymerization Functionalization, Charge Transport, Conductive Polymers, PEDOT

ABSTRACT: Herein, a route to produce highly electrically conductive doped hydroxymethyl functionalized poly(3,4-ethylenedioxythiophene) (PEDOT) films, termed PEDOT(OH) with metallic charge transport properties using a fully solution processable precursor polymer is reported. This is achieved via an ester-functionalized PEDOT derivative [PEDOT(EHE)] that is soluble in a range of solvents with excellent film-forming ability. PEDOT(EHE) demonstrates moderate electrical conductivities of 20-60 S cm^{-1} and hopping-like (*i.e.,* thermally activated) transport when doped with ferric tosylate ($FeTos_3$). Upon basic hydrolysis of PEDOT(EHE) films, the electrically insulative side chains are cleaved and washed from the polymer film, leaving a densified film of PEDOT(OH). These films, when optimally doped, reach electrical conductivities of ~1200 S cm^{-1} and demonstrate metallic (*i.e.,* thermally deactivated and band-like) transport properties and high stability at comparable doping levels.

Introduction

Following the development of the 3,4-ethylenedioxythiophene (EDOT) monomer and its homopolymer, PEDOT, by Bayer in the late 1980s,[1],[2] this material and its derivatives have been among the most studied and commercialized conjugated polymers (CPs). Initially, PEDOT, shown in Scheme 1a, was designed for improved handling, oxidative dopability, and stability compared to poly(pyrroles) and poly(thiophenes).[2],[3] Over the past 30 years, PEDOT, as well as PEDOT derivatives/analogs, have found utility in a wide range of developing applications and is currently used commercially in electrolytic capacitors and as anti-static coatings.[4],[5],[6],[7] Of the numerous desirable properties of PEDOT for both solid-state[8],[9] and in situ electrochemical[10] applications, its high and stable solid-state electrical conductivity (σ) when oxidatively doped is likely the most important. Unfortunately, the tradeoff of these exceptional properties is processability, with PEDOT being completely insoluble and typically directly electrochemically polymerized onto a current collector. A significant amount of work has been devoted to optimizing the electrochemical polymerization conditions for tuning the optical, electrochemical, and morphological properties.[10],[11] ,[12],[13] Introduction of solubilizing hydrocarbon or oligoether side chains to yield a processable "soluble PEDOT" has historically resulted in oligomers or polymers with notably different properties (e.g., bandgap, onset of oxidation, etc.) than PEDOT, likely due to low molecular weight or steric interactions.[14],[15] While our focuses is on solution processing of PEDOTs, we note that oxidative molecular layer deposition (OMLD)[16] and oxidative chemical vapor deposition (oCVD)[17] methods can provide high σ and conformal PEDOT-based films with excellent thickness control, provided the specialized setups are available and compatible with the substrates of interest.

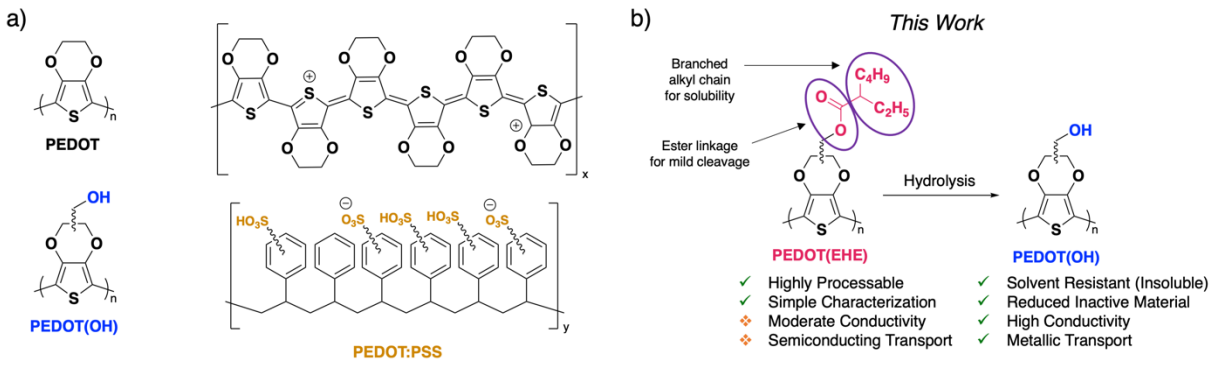

Scheme 1. A) Lewis structures of the homopolymers PEDOT and PEDOT(OH), along with PEDOT:PSS. B) Structure of the functionalized PEDOT homopolymer, PEDOT(EHE), that can be converted to PEDOT(OH) upon hydrolysis of the side chains.

The insolubility of PEDOT can be circumvented by forming a dispersion of doped PEDOT chains with a charge balancing and solubilizing surfactant, with sulfonated poly(styrene) in water being the most commonly used. This material, poly(3,4-ethylenedioxythiophene):poly(styrene sulfonate) (PEDOT:PSS, shown in Scheme 1a), has become ubiquitous in the field of Org. Electron., serving as both an active material for numerous applications and as interlayers in many devices. Importantly, PEDOT:PSS can serve as a flexible electrode[18] for electrochromism,[19] organic photovoltaics,[20] and supercapacitors,[21] along with serving as a hole transport layer for perovskite solar cells.[22] Despite the many successes of PEDOT:PSS, challenges remain when using this material, primarily resulting from a poor understanding of the materials' composition and structure,[23] the secondary solution treatments and additives needed to obtain highly conductive films,[19],[24],[25] and the residual strongly acidic protonated sulfonate groups in the PSS that can corrode other components in devices.[26]

Hydroxymethyl-functionalized PEDOT [referred to as PEDOT(OH) in this text and shown in Scheme 1a], first synthesized in the early 2000s via an EDOT(OH) monomer with higher water-solubility compared to EDOT,[27] has gained increased attention in recent years due to its versatility in a range of redox-, bio-, and energy-related applications. Introduction of the polar alcohol functionality to the polymer backbone increases aqueous compatibility (as seen by improved film wetting[28]) and allows for highly stable redox switching in salt water electrolyte-based supercapacitors.[29] Films of PEDOT(OH) have been used as biocompatible electrodes and organic

bioelectronic interfaces, with PEDOT(OH) films having been found to reduce impedance on multichannel neural probes,[30] offer improved cell adhesion and viability compared to uncoated substrates,[31],[32] and provide electrical stimulation for neurite outgrowth when doped with tosylate (Tos).[33] In addition to these biological applications, PEDOT(OH) has been used in quantum dot-sensitized solar cells[34] and as the hole transport material in perovskite solar cells.[35] However, preparation and deposition of this polymer often relies on electropolymerization or chemical polymerization *in-situ,* yielding materials which are not easily characterized and have limited device application due to the constraints of these preparation methods.

Side chain removal following solution processing has been demonstrated using several methods of cleavage (e.g., thermal-,[36] photo-,[37] base-induced[38]) for various structures and targeted applications. Building off the work of Reeves and coworkers,[38] we have reported that, post-processing removal of ester-based side chains via basic hydrolysis significantly increases the σ of CP films.[39] Upon hydrolysis, the cleaved side chains (now carboxylate salts in solution) are removed from the film, leading to overall mass loss and volumetric contraction due to denser packing of the remaining minimally substituted conjugated backbones. This results in solvent resistant polymer films with a higher density of electroactive material compared to the ester functionalized precursor polymer. The films show lower onsets of oxidation (E_{ox}), higher σ (up to 11-fold increases), and lower Seebeck coefficients (S) compared to their parent ester polymers. Using a combination of measurements, it was determined that the increased σ and decreased S are due to an increased charge carrier density resulting from a similar number of charge carriers populating a smaller volume in the contracted solvent resistant films.

Herein, we detail a route to highly electrically conductive PEDOT(OH) films via a solution processable precursor polymer. We report the synthesis of a 2-ethylhexyl ester side chain functionalized PEDOT homopolymer, termed PEDOT(EHE), that is highly soluble in typical organic solvents. Application of our previously reported film hydrolysis method[39] converts films of this soluble material to solvent resistant films of PEDOT(OH), as shown in Scheme 1b and in more detail in Scheme S1. Doping films of PEDOT(EHE) with ferric tosylate ($FeTos_3$) results in moderate σ values of 18-65 S cm^{-1}, depending on processing conditions. In comparison, PEDOT(OH) films, obtained via hydrolysis of PEDOT(EHE) films, show exceptionally low E_{ox}

values and high σ (~300 S cm^{-1}) from air-doping in ambient conditions. Further doping of PEDOT(OH) films with $FeTos_3$ or $FeCl_3$ results in σ ranging from 680-1200 S cm^{-1}, depending on doping concentration. Seebeck coefficient measurements, volumetric film contraction, X-ray photoelectron spectroscopy (XPS), and grazing-incidence wide-angle X-ray scattering (GIWAXS) are used to explain these differences in electrical conductivity. Finally, temperature-dependent measurements are used to examine the change in transport mechanism upon hydrolysis, with doped PEDOT(EHE) showing thermally activated (localized, hopping) transport and PEDOT(OH) showing thermally deactivated (delocalized, metallic) transport. This study outlines a material and method that allows for both typical solution processing and exceptionally high electrical conductivity with metallic transport properties.

Results and Discussion

Synthesis

The synthetic pathways to the EDOT derivatives used in this work are outlined in Figure S1 and are briefly discussed here, with full synthetic and characterizations details in the Supporting Information. The ester functionalized EDOT monomers were prepared, as shown in Figure S1, starting from 3,4-dimethoxythiophene and (±)-3-chloro-1,2-propanediol to form EDOT(CH_2Cl) as a mixture of (±) enantiomers. This species was then alkylated via an S_N2 reaction with (±)-2-ethylhexanoic acid to form the EDOT(EHE) monomer. Halogenation of this monomer, yielding EDOT(EHE)-Br_2, was achieved by electrophilic bromination.

PEDOT(EHE) was prepared via direct heteroarylation polymerization (DHAP) using an adapted version of the polar DHAP conditions found to be effective for XDOTs,[40] as shown in Figure 1, and employing a recently developed temperature ramp found to produce larger molar mass polymers with highly reactive EDOT-based monomers.[41] The polymer composition was confirmed by elemental analysis, the repeat unit structure was confirmed by proton NMR, and the molecular weight (M_n = 10.9 kg/mol, $Đ$ = 1.2) was estimated by chloroform GPC relative to polystyrene standards, with full synthetic details reported in the Supporting Information. Matrix-assisted laser desorption/ionization-time of flight (MALDI-TOF) mass spectrometry was used to provide further confirmation of the polymer structure, with peaks corresponding to expected chain masses in intervals consistent with the repat unit mass, with no Br end groups being observed.

PEDOT(EHE) was isolated as a blue/black solid with a gold, metal-like reflection, as seen in Figure S2. To assess the reproducibility of the synthesis of this polymer and its resulting properties, a second polymerization was set up using a slightly different experimental setup, as detailed and discussed in the Supporting Information, and yielded a second batch of PEDOT(EHE) nearly identical to the first batch in terms of molecular weight (M_n = 11.3 kg/mol, $Đ$ = 1.3) and purity.

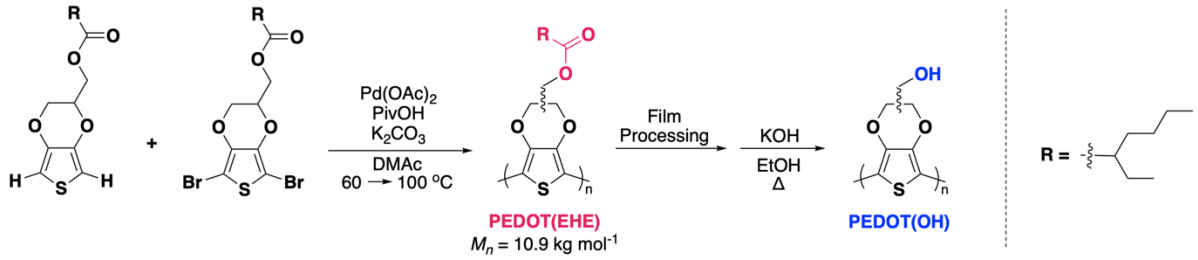

Figure 1. Synthetic approach to the alkyl ester functionalized PEDOT homopolymer, PEDOT(EHE), and subsequent hydrolysis of polymer films to PEDOT(OH).

As a result of the branched side chains on every EDOT ring, the polymer is soluble in a range of organic solvents (e.g., chloroform, toluene, hot THF, etc.). It should be noted this polymer is both atactic and regiorandom, illustrated in Figure S3, due to the mixture of (±) isomeric monomers and lack of selectivity between the 2- and 5-positions of the EDOT ring during polymerization. Thermogravimetric analysis (TGA, Figure S4a) indicates that the ester polymer is thermally stable to ~320 ˚C, and by differential scanning calorimetry (DSC, Figure S4b), no distinct thermal transitions are observed between -50 ˚C and 300 ˚C, as expected based on the previously discussed disordered nature of the side chains.

Film Processing and Post-Processing

Thin films (see Figure S5a) of PEDOT(EHE) were prepared by blade-coating concentrated solutions (15-30 mg mL^{-1}) onto substrates (either borosilicate glass or undoped silicon) at different blade speeds and heights over the substrate to control film thickness (generally producing PEDOT(EHE) films 0.8-1.2 μm thick). Typical films for transport measurements were cast from a 4:1 chloroform/chlorobenzene solution on 1x1 cm glass substrates, as detailed and discussed in the Supporting Information.

Initially, our previously reported[39] hydrolysis conditions were used for preparation of these films; however, many of the PEDOT(EHE/OH) films delaminated (peeled partially/completely off the glass substrate) using these unoptimized and relatively harsh conditions. Consequently, to access films for this study, several alternative hydrolysis conditions were tested, and a new mild procedure was developed that yielded the same effective side chain removal and increased electrical conductivity, but without film delamination, as discussed in detail in the Supporting Information. Photographs of hydrolyzed films of PEDOT(OH) and the hydrolysis setup are shown in Figures S5b and c, respectively.

Upon hydrolysis of PEDOT(EHE), the cleaved carboxylate salt-terminated hydrocarbon chains dissolve into the bulk solution, leading to a volumetric contraction of the resulting solvent resistant PEDOT(OH) films, as previously observed.[39] As seen in Figure S6 for a representative sample, optical profilometry maps of several samples show a volumetric reduction of 51 ± 2 % going from PEDOT(EHE) to PEDOT(OH) in thick (0.8 and 1.2 μm) polymer films. The larger volumetric change relative to the expected mass change (43%, based on side chain molecular weight and assuming full side chain removal) is likely due to the higher density of the minimally functionalized aromatic backbones (e.g., crystalline PEDOT, 1.47 g cm^{-3})[42] relative to hydrocarbon functionalized polymers (e.g., P3HT, 1.10 g cm^{-3}).[43] Additionally, the hydrolysis and introduction of polar alcohol functionalities in the film results in a decrease in the water contact angle (see Figure S7), with a reduced contact angle for the cleaved polymer (59°) compared to the parent ester polymer (78°).

Charge Transport Properties and Doping Level

The solid-state electrical properties (σ and S) of blade-coated PEDOT(EHE/OH) films were evaluated using a four-point Van der Pauw method and temperature-controlled Peltier stages. As-cast films of PEDOT(EHE) show no appreciable conductivity, as expected for an undoped polymer film. Surprisingly, as-hydrolyzed PEDOT(OH) films that have been exposed to an ambient atmosphere have relatively high σ values of 325 ± 48 S cm^{-1} and moderate S values of +33 ± 2.9 μV K^{-1} without any additional chemical doping or anion exchange. This suggests that the films are doped by air during the hydrolysis and/or drying process (additional details and discussion of doping under ambient conditions can be found in the Supporting Information). Sulfur XPS

analysis, as seen in Figure S8 and discussed in the Supporting Information, of the as-hydrolyzed films indicate a doping level (*i.e.,* extent of oxidation or the carrier ratio) of 0.28 ± 0.06 charges per EDOT ring (approximately one charge per 3-4 EDOT rings), consistent with computational work showing a minimum Gibbs energy for PEDOT at a doping level of 0.33, independent of the anion.[44] Treatment of these films with hydrazine [0.15 M in acetonitrile (ACN) for 1 minute] resulted in a reduction of the σ values to 130 ± 42 S cm^{-1}, with a corresponding increase in *S* values to +43 ± 4.4 μV K^{-1}, indicating partial, but incomplete, de-doping of the polymer films and suggesting a high level of stability in the doped state.

Solution doping of PEDOT(EHE/OH) films with 50 mM $FeTos_3$ in ACN was used as a first test to assess the transport properties of these materials, with the resulting σ and *S* values shown in Figure 2a. Doping of PEDOT(EHE) results in modest σ values of 18.5 ± 5.5 S cm^{-1}, with corresponding *S* values that are exceptionally low, on the order of +11 μV K^{-1}, compared to many other CP systems, but are similar to those reported for dioxy-substituted heterocycles[39],[45],[46] which attain high doping levels. PEDOT(OH) films doped in a comparable way yield significantly higher σ values of 695 ± 88 S cm^{-1}. The *S* values of this PEDOT(OH) system are even lower and metal-like, on the order of +2 μV K^{-1}. Reproducibility of this system and methodology was demonstrated by processing and measuring films of a second batch of PEDOT(EHE) in the same way as previously discussed. As seen in Figure S9, the excellent agreement in σ and *S* values between polymer batches, both for the moderately conductive ester films and the highly conductive solvent resistant films, illustrate the reproducibility of this polymer system and post-processing method. Based on these results, the two polymer batches are used interchangeably for other experiments presented here.

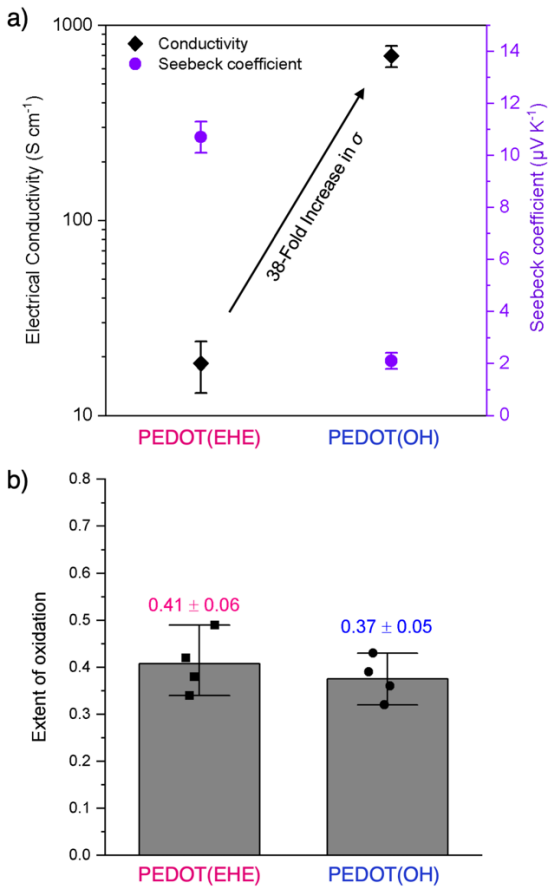

Figure 2. a) Electrical conductivity and Seebeck coefficients of blade coated PEDOT(EHE) and PEDOT(OH) doped using 50 mM $FeTos_3$/ACN. Error bars represent sample-to-sample standard deviation. b) Extent of oxidation for PEDOT(EHE) and PEDOT(OH) films doped with 50 mM $FeTos_3$/ACN, as determined by XPS analysis. Error bars represent sample-to-sample standard deviation in the calculated area ratios for oxidized thiophene and tosylate counter-ion of two unique samples.

We now consider the origin of the σ increase and S decrease in the PEDOT(EHE/OH) system, which is a notably larger change in σ (~38-fold) compared to our previous ProDOT-based model.[39] The increase in σ is intuitive: removal of the insulative side chains results in a larger volume fraction of conductive domains. Conversely, the decrease in S is less obvious, as the value of S is less dependent on microstructure; rather, S is anticorrelated with the carrier density and with the symmetric filling of frontier electronic states. Therefore, to determine the decrease in S between 50 mM $FeTos_3$ doped PEDOT(EHE) and PEDOT(OH) films, we employed X-ray photoelectron spectroscopy (XPS) to quantify doping level and carrier density. Discussions of the XPS measurements and deconvolution procedures are detailed in the Supporting Information. Sulfur

(2p) XPS spectra were collected for PEDOT(EHE) and PEDOT(OH) films in their pristine (as-cast/as-hydrolyzed) and 50 mM $FeTos_3$ doped states, with representative spectra shown in Figure S8. Deconvoluting these spectra, we calculate that the doping level in the 50 mM $FeTos_3$ doped states for both PEDOT(EHE) and PEDOT(OH) is ~ 0.4 (see Figure 2b), indicating two charges distributed across five EDOT rings. Therefore, with this analysis, we conclude that the extent of chemical doping is effectively independent of the side chain chemistry, and the extent of doping is not responsible for the differences in Seebeck coefficients. However, optical profilometry maps taken of the films (Figure S6) show that hydrolysis contracts the thickness and volume of the film by ~50%, as previously discussed. Therefore, based on the comparable extents of oxidative doping, but ~50% thinner films, we calculate that the 50 mM $FeTos_3$ PEDOT(OH) films have a carrier density of 1.3 (± 0.2) × 10^{21} carriers cm^{-3}, which is ~50% larger than that for comparably doped PEDOT(EHE) films [0.83 (± 0.1) × 10^{21} carriers cm^{-3}] (see the Supporting Information for additional notes on the calculation methodology). Ultimately, these XPS and optical profilometry measurements indicate that the hydrolysis procedure increases the volumetric charge carrier density, which is consistent with the decrease in the Seebeck coefficient, as proposed and discussed in more detail in our previous report.[39]

Electrochemical and Optical Properties

To better understand the large changes in charge carrier density and transport following side chain cleavage, we turn to probing the electrochemical and optical properties of the PEDOT(EHE/OH) system. Electrochemical analysis was used to assess changes in the electron richness of the PEDOT(EHE/OH) system before and after hydrolysis, providing insight into the effectiveness of doping these species. 1-Ethyl-3-methylimidazolium tosylate (EMITos) was selected as the electrolyte salt to provide a matching anion to that from $FeTos_3$ dopant in solid-state experiments. Cyclic voltammetry (CV, Figure 3) measurements of polymer films on glassy carbon button electrodes show broad electrochemical responces and low E_{ox} values, as expected from polymers with a high EDOT content.[3],[47] We observe significant changes (i.e., differences in peak current density, peak location, onset of oxidation) in the electrochemical response of the polymer films following side chain cleavage, consistent with previous studies.[39],[48] The E_{ox} values of the polymer films before and after cleavage were monitored by differential pulse votammetry (DPV), as seen in Figure S10. While PEDOT(EHE) has an E_{ox} (-0.67 V vs. Fc/Fc^+) comparable to

previously reported soluble PEDOT analogs,[47] PEDOT(OH) has an exceptionally low E_{ox} of -1.33 V vs. Fc/Fc^+, significantly lower than any other polymer we have observed. It is believed this low E_{ox} is the underlying cause of the significant doping under ambient conditions of PEDOT(OH), and consistent with other observations of the spontaneous oxidation of EDOT-rich polymers.[49]

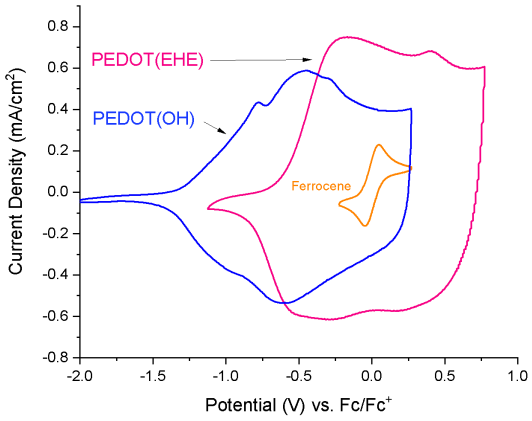

Figure 3. Cyclic voltammograms of a drop cast PEDOT(EHE/OH) film before and after hydrolysis, on a glassy carbon button in a 0.1 M EMITos/PC electrolyte solution using an Ag/AgCl reference electrode (427 mV vs Fc/Fc^+) at a scan rate of 50mV/s.

Additionally, E_{ox} value for PEDOT(OH) films processed from our soluble precursor (-1.44 V vs. Fc/Fc^+, Figure S11) are lower than reported values for electropolymerized films of PEDOT(OH) (~ -0.93 V vs. Fc/Fc^+)[27],[50] or unfunctionalized PEDOT (-1.0 V vs. Fc/Fc^+)[47] measured in the same electrolyte [tetrabutylammonium hexafluorophosphate ($TBAPF_6$)]. While all three systems have the same conjugated polymer backbone, the relatively low E_{ox} value of PEDOT(OH) resulting from this method is hypothesized to be due to improved microstructure of the solution-cast films (e.g, potentially better chain extension) versus the electropolymerized films and/or a relatively higher degree of polymerization; however, further investigation is needed to elucidate differences in E_{ox} film values prepared by either solution-processing or electropolymerization.

The effects of side chain cleavage and/or doping on PEDOT(EHE/OH) films were monitored in the solid-state using UV-vis-NIR measurements on glass substrates, as seen in Figures 4a and 4b. In the pristine/as-cast state of PEDOT(EHE), the charge neutral π-π* transition (300-700 nm) is

primarily observed, with only trace polaronic absorbance (700-1200 nm). In contrast, the pristine/as-hydrolyzed state of PEDOT(OH) shows a nearly depleted π-π* transition and large charge carrier band absorbances across the near-IR, suggesting an "intrinsic" change in electrochemical properties.[51] Treatment of the films with a hydrazine solution effectively dedoped PEDOT(EHE), as seen by suppression of the previously mentioned polaronic absorbance. However, hydrazine was ineffective at causing any notable change in the absorbance of PEDOT(OH) films due to the low E_{ox} of these films, as consistent with previously discussed transport measurements on pristine (as-hydrolyzed) films in section 2.3. $FeTos_3$ (50 mM in ACN) doping of PEDOT(EHE) leads to a complete loss of the π-π* absorbance and formation of a broad bipolaron band. Similarly, $FeTos_3$ doping of PEDOT(OH) under the same conditions bleaches the residual π-π* absorption and produces a bipolaron band. Further discussion of the hydrazine treatment and doping methodology can be found in the Supporting Information.

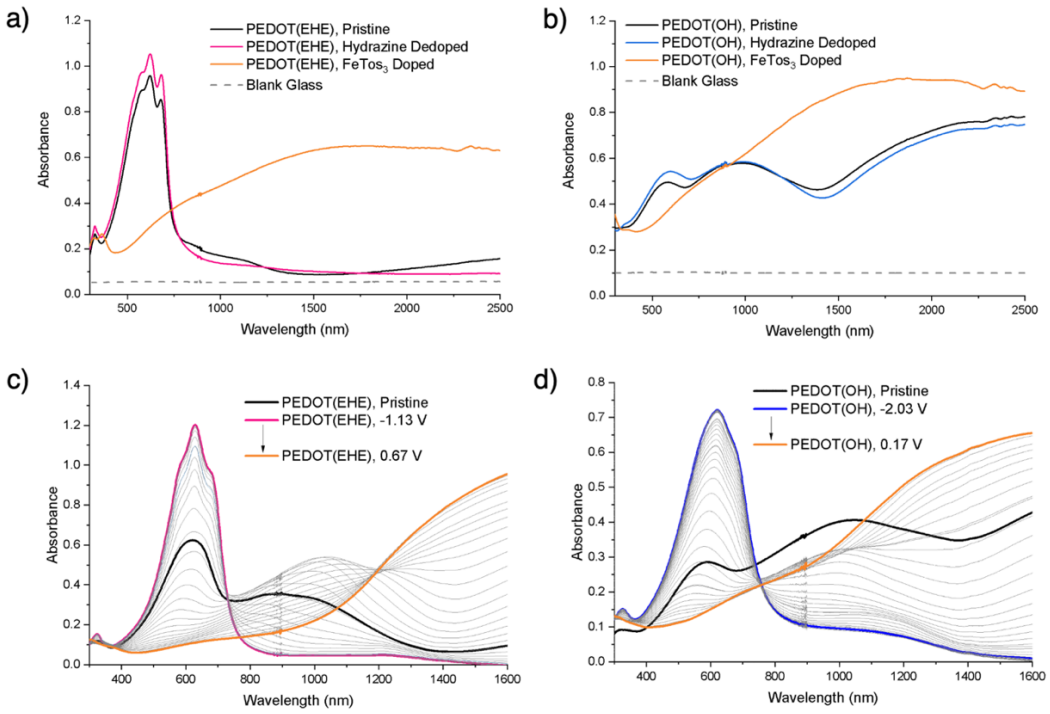

Figure 4. UV-vis-NIR spectra of blade coated a) PEDOT(EHE) and b) PEDOT(OH) films on glass in the pristine (as-cast or as-hydrolyzed), hydrazine dedoped, and $FeTos_3$ doped (50 mM in ACN) states. Spectroelectrochemistry of spray cast c) PEDOT(EHE) and d) PEDOT(OH) films on ITO glass electrodes using the same cell conditions as CV/DPV experiments. Potentials reported vs. Fc/Fc^+. Full details on both experiments are outlined in the Supporting Information.

As PEDOT(OH) films could not be dedoped using conventional reducing agents, spectroelectrochemistry was utilized to observe the evolution of charge carrier bands in polymer films as a function of doping, with EMITos again serving as an electrolyte to provide a consistent anion species across measurements. The PEDOT(EHE) was spray cast onto ITO glass and then either used directly or hydrolyzed to form PEDOT(OH). In Figure 4c, we note that pristine PEDOT(EHE) has an obvious polaron peak in the near-IR in its pristine state, consistent with spectra of EDOT-containing polymers processed via spray-coating due to the increased exposure of polymer chains to air.[49] Following electrochemical conditioning (also termed "break-in"),[52],[53] the films were reduced to their charge neutral (reduced) states and then oxidized stepwise with increasing potentials to the fully doped (oxidized) states. For PEDOT(EHE), increasing the potential causes gradual loss of the π-π* transition with concomitant appearance of charge carrier bands in the near-IR, as seen in Figure 4c. Polaronic absorbances, centered around 1000 nm, seen at intermediate potentials, are then fully converted to a bipolaron band absorbance at higher doping levels. The resulting fully doped films are colorless to the eye (Figure S12) in agreement with spectra (Figure 4) showing transmission across the visible and absorption in the near-IR. While application of a large negative potential was able to significantly dedope PEDOT(OH) films, as seen in Figure 4d, residual polaronic absorbance at ~900-1300 nm indicates the presence of residual charge carriers. Direct comparison of the neutral (reduced) state PEDOT(EHE) and PEDOT(OH) spectra (Figure S13a) shows little change in optical bandgap and λ_{max}. In the oxidized state of these films (Figure S13b), however, polaron and bipolaron absorptions are dissimilar with regards to peak location and shape. Potentials used to reach equivalently oxidized states also differ [e.g., 0.17 V vs. Fc/Fc^+ for PEDOT(OH) versus 0.67 V vs. Fc/Fc^+ for PEDOT(EHE) to reach the bipolaronic state]. Ultimately, these observations allude to differences in the density of electronic states and/or oscillator strengths (i.e., extinction coefficients) for the PEDOT(EHE/OH) system based on side chain cleavage.[54],[55]

Charge Transport Optimization

We now turn to optimizing processing and doping parameters to increase the σ of PEDOT(EHE/OH) films, focusing primarily on PEDOT(OH). Specifically, solvent selection, thermal annealing, dopant chemistry, and dopant molarity are investigated. Figure S14 shows the

resulting σ of PEDOT(OH) films (doped with 50 mM $FeTos_3$) cast from various solvents, including chloroform ($CHCl_3$), chlorobenzene (CB), tetrahydrofuran (THF), toluene (Tol), and a test "green" solvent system, 2-methyl tetrahydrofuran (2-MeTHF).[56] Halogenated solvents ($CHCl_3$ and/or CB blends) yielded slightly higher average σ (~650 S cm^{-1}); however, there is no statically significant change observed in σ when changing solvent. We attribute these slight changes in σ and sample to sample variation to chlorinated solvents more effectively dissolving the polymer and producing smoother films, with the 4:1 $CHCl_3$/CB solvent system selected for further experiments as it produced the highest quality films, likely resulting from optimal drying rates. We next examine whether thermal annealing could further increase the electrical conductivity. For PEDOT(OH), thermal annealing at 100 °C, before or after doping, did not lead to any change in σ. Thermal annealing of PEDOT(EHE) prior to doping similarly yielded no observable electrical conductivity changes. In contrast, thermally annealing PEDOT(EHE) films at 100 °C following doping leads to an irreversible ~3-fold increase in σ (65 ± 11 S cm^{-1}) with essentially no change in S (9.6 ± 3.4 μV K^{-1}), as seen in Figure S15.

Next, we turned to varying the dopant chemistry, while holding the 50 mM doping solution concentration constant. Figure S16 shows the σ values for PEDOT(OH) films doped with $FeCl_3$, ferric triflate, $AgPF_6$, $KAuCl_4$, F4TCNQ, $NOPF_6$, and tris(4-bromophenyl)ammoniumyl hexachloroantimonate (Magic Blue), along with the $FeTos_3$ results. At this molarity, most dopant chemistries yielded comparable or lower electrical conductivities compared to $FeTos_3$ tosylate and similar S values. $FeCl_3$ is a notable exception, yielding an average σ of ~850 S cm^{-1}, but the substantial overlap in sample-to-sample error with the $FeTos_3$ precludes a more robust claim of increased σ using this dopant.

Lastly, with both the $FeCl_3$ and $FeTos_3$ dopant systems, we systematically varied the dopant solution molarity in ACN. Although 50 mM solutions have yielded high electrical conductivities in other XDOT-based systems, we recognize that excessively high dopant molarities can lead to lower electrical conductivities in some polymer systems.[57] Figure 5a shows the electrical conductivities for PEDOT(OH) films doped with 1, 5, 10, and 50 mM solutions of either $FeCl_3$ or $FeTos_3$. In general, we find that PEDOT(OH) films obtain optimized σ values averaging ~1,100 S cm^{-1} when doped with 5-10 mM solutions, while undershooting or overshooting the dopant

solution concentration (i.e., 1 and 50 mM $FeTos_3$) yielded lower σ ranges, 600-800 S cm^{-1}. This demonstrates the importance of doping optimization, as materials could be easily dismissed based on unoptimized results. All films show low Seebeck coefficients (less than +10 $\mu V\,K^{-1}$), independent of dopant chemistries and concentration, indicating comparable carrier densities. Therefore, the extent of doping is not primarily responsible for these changes in electrical conductivity, and deeper microstructural examination is needed.

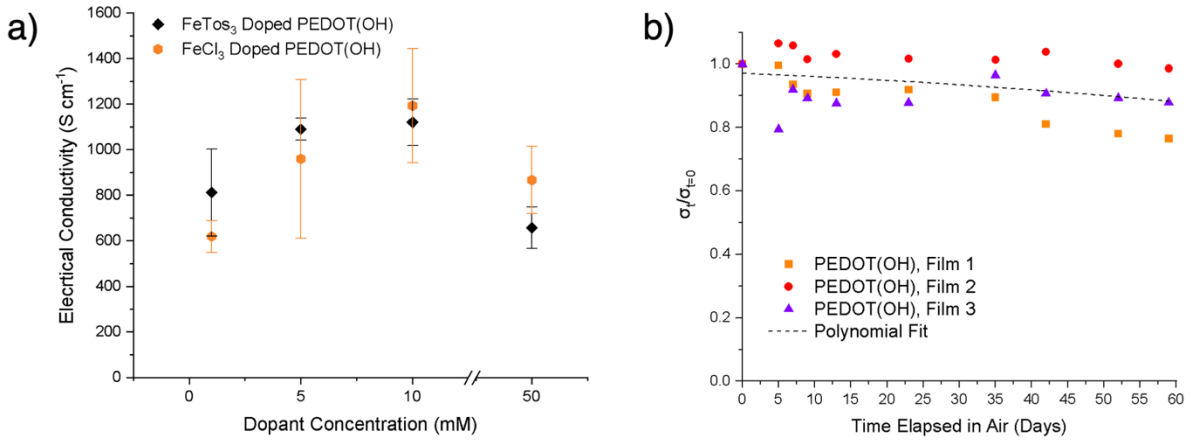

Figure 5. a) Electrical conductivity of PEDOT(OH) films doped with either $FeTos_3$ or $FeCl_3$ at various concentrations in ACN. Error bars represent sample-to-sample standard deviation. b) Electrical conductivities as a function of time for three unique PEDOT(OH) films doped with $FeTos_3$ at 10 mM. Conductivities plotted as the ratios of the electrical conductivity at a given time (σ_t) per the electrical conductivity when first doped ($\sigma_{t=0}$). A polynomial trend line is shown to illustrate the trend in conductivity over time.

We note that the σ of these films are highly stable over time in air, as expected by the significant degree of ambient doping and high σ following hydrolysis. Shown in Figure 5b, films of 10 mM $FeTos_3$ doped PEDOT(OH) retain their σ after weeks of exposure to ambient lab conditions. This stability, comparable to other highly doped PEDOTs, is significantly higher than many commonly studied conductive polymers. For example, the σ of PBTTT films drops in a matter of hours in air, with a nitrogen atmosphere only extending this to several days.[58]

X-Ray Morphological Analysis

Grazing-incidence wide-angle X-ray scattering (GIWAXS) was employed to further quantify and understand how microstructural changes may contribute to the observed differences in σ values.

The two-dimensional diffractograms for PEDOT(EHE) and PEDOT(OH) at various $FeTos_3$ doping and annealing conditions can be seen in Figures S17, with additional discussion of these results found in the Supporting information. From the diffractograms, pristine PEDOT(EHE) exhibits a mix of face-on and edge-on orientations for the lamellar and a preferred face-on orientation for the π-π stacks. After hydrolysis, pristine PEDOT(OH) presents a preferred face-on lamellar orientation and a more isotropic π-π stacking orientation, resembling PEDOT.[59],[60] As extracted from the radially integrated diffractograms, pristine PEDOT(EHE) has lamellar spacing peaks centered at 0.30 $Å^{-1}$ and 0.38 $Å^{-1}$ (*d*-spacing of 20.9 and 16.5 Å), corresponding to the mixed orientations, and a π-π spacing peak at 1.74 $Å^{-1}$ (d-spacing of 3.61 Å). Side-chain removal results in the lamellar spacing decreasing to 12.6 Å and the π-π spacing decreasing to 3.52 Å in as-hydrolyzed PEDOT(OH), a comparable value to previous reports of PEDOT[59],[60] doped with tosylate counterions. This huge decrease in lamellar spacing and smaller change in π-π spacing clearly shows that removing side-chains decreases the distance between the polymer chains in all directions, and this is consistent with the notable increase in electrical conductivity. Doping and annealing of PEDOT(EHE/OH) films result in relatively small changes in π-π spacing, as shown in Table S1; however, there are significant changes in the lamellar spacing. When doped with 50 mM $FeTos_3$, the PEDOT(EHE) lamellar peak at 20.9 Å narrows, indicating a greater extent of side-chain ordering, as shown in Table S2. The second lamellar peak shifts from 16.5 to 17.5 Å, indicating some dopant intercalation between lamellae. Additionally, new peaks near 11.4 and 12.6 Å (0.50 and 0.55 $Å^{-1}$) emerge with similar orientation to the lamellar, which we ascribe to ordered tosylate rich domains. After annealing, these tosylate peaks become more ordered, as seen by the lower peak widths. Additionally, a third population emerges at 15.0 Å (0.42 $Å^{-1}$), potentially indicating further dopant intercalation and consistent with the increase in conductivity. A distinct trend is observed in PEDOT(OH) as a function of doping. Upon doping, the lamellar spacing incrementally increases from 12.6 Å in pristine PEDOT(OH) to 21.7 Å in PEDOT(OH) doped with 10 mM $Fe(Tos)_3$, indicating that tosylate anions are gradually intercalating between PEDOT(OH) lamellae. At 50 mM, the lamellar spacing decreases to 16.5 Å, broadens, and exhibits the same features found in 50 mM doped PEDOT(EHE) that we ascribe to tosylate-rich domains. These broad and defect-rich lamellar peaks indicate lower extents of ordering in PEDOT(OH) doped with 50 mM $FeTos_3$ compared to the 10 mM doped films, consistent with trends in electrical

conductivity. Ultimately, these changes in microstructural spacings help contextualize the large changes in transport properties as a function of side chain chemistry and extent of doping.

To better examine the ordering quality of the π-π stacks, paracrystallinity ($g_{\pi\text{-}\pi}$) was calculated for the (020) peak of PEDOT(EHE) and PEDOT(OH) films as a function of doping level and/or annealing, as summarized in Table S1 and shown in Figure S18. Pristine PEDOT(EHE) has the highest $g_{\pi\text{-}\pi}$-value of ~ 13%, where a high $g_{\pi\text{-}\pi}$ indicates a greater extent of disorder.[61] Doping PEDOT(EHE) slightly decreases *g* to 12%, and subsequent annealing leads to further reduction to 11%. This increase in order upon annealing explains the previously noted increase in σ upon annealing as the minimal change in *S* suggests little to no change in charge carrier density. Compared to pristine PEDOT(EHE), as-hydrolyzed PEDOT(OH) exhibited a similar $g_{\pi\text{-}\pi}$ of 13%. Upon doping, *g* progressively decreases with increasing dopant concentration (1 to 50 mM $FeTos_3$) for PEDOT(OH) to 12%, indicating that doping increased the ordering of the π-π stacks of PEDOT(OH). These low *g* values of doped PEDOT(EHE) and PEDOT(OH) films are consistent with a classification between 2D and 3D semi-paracrystallinity.[61] Additionally, these $g_{\pi\text{-}\pi}$ values place this system closer to the more ordered polymers PBTTT ($g_{\pi\text{-}\pi}$ ~ 9%, PF_6 counterions) and P3HT ($g_{\pi\text{-}\pi}$ ~ 11%, PF_6 counterions) than the lower order polymers like IDT-BT ($g_{\pi\text{-}\pi}$ ~ 24%, PF_6 counterions),[62] despite the random orientation of the side chains/alcohol units. Interestingly, while the σ of PEDOT(OH) is ~20-fold higher than annealed PEDOT(EHE), the corresponding $g_{\pi\text{-}\pi}$-values are comparable (12% vs. 11%). This is in stark contrast to recent reports of a correlation between higher paracrystalline order and higher electrical conductivities.[62] We note that while a reduction in statistical fluctuation between π-π stacks (lower $g_{\pi\text{-}\pi}$-values) may generally contribute to an increase in observed transport within a given structural motif (e.g, alkyl functionalized CPs), this trend cannot account for the significant changes induced by side chain cleavage and is only informative regarding the crystalline portion of the film and provides little information about the bulk amorphous phase nor macroscopic ensemble.

Temperature-Dependent Transport

Here, we turn to examining the temperature-dependent electrical conductivity, $\sigma(T)$, for various PEDOT(EHE) and PEDOT(OH) films as $\sigma(T)$ can provide deeper insights on the transport mechanisms that are most responsible for the observable electrical conductivity at a static

temperature, a topic further discussed in terms of fundamental principles in the Supporting Information. Figure 6 shows the normalized electrical conductivity as a function of temperature for 50 mM $FeTos_3$ doped PEDOT(EHE) after thermal annealing and PEDOT(OH) doped with $FeTos_3$ at 5, 10, and 50 mM $FeTos_3$; additionally, Figure S19 shows the nominal electrical conductivities. $\sigma(T)$ measurements for the PEDOT(EHE) films are thermally activated, with an Arrhenius-like activation energy of 20 meV, as is expected from hopping-like transport. In contrast, $\sigma(T)$ measurements of PEDOT(OH) films show thermal deactivation, a feature more consistent with metallic-like transport. This decrease in activation energy with concomitant decrease in Seebeck coefficient is consistent with both our previous reports on cleavable ProDOT-based systems and the semi-localized transport (SLoT) model.[39],[63] Furthermore, the extent of thermal deactivation (i.e., the steepness of the downward slope in Figure 6) is indicative of how metallic the system behaves. We find that as the nominal σ at 20 °C increases, the slope decline increases in magnitude for these doped PEDOT(OH) films. A similar and more pronounced metallic trend, as σ increases $\left|\frac{d\sigma}{dT}\right|$ also increases, is also observed as a function of dopant chemistry, as seen in Figure S20. For the 5-50 mM doped samples, there is essentially no change in the σ value upon returning to room temperature, as seen in Figure S19a, indicating the heating is not changing the morphology or doping level of the PEDOT(OH) films. Alternatively, the 1 mM doped samples show a drop in σ after heat, indicating some irreversible process, seen in Figure S19b.

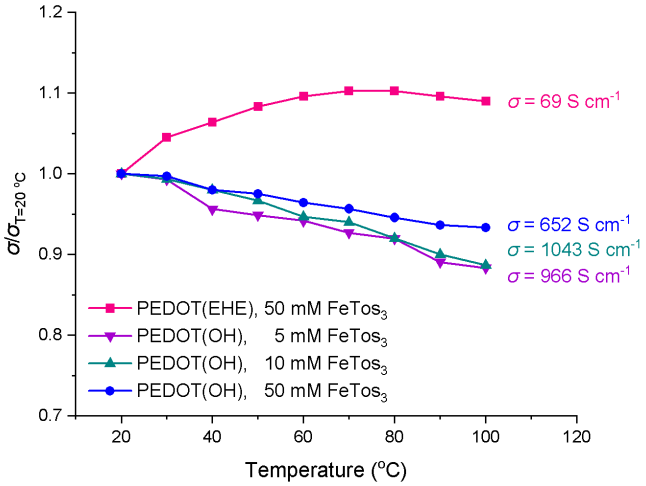

Figure 6. Relative change in electrical conductivity as a function of temperature for representative PEDOT(EHE) and PEDOT(OH) (various doping levels) films. The PEDOT(EHE) film was doped using 50 mM $FeTos_3$ and thermally annealed, as previously described, with a resulting σ of 63 S cm^{-1} at 20 °C (for this specific film). PEDOT(OH) films were doped to various doping levels, as outlined in Figure 5, with σ values at 20 °C (for these specific films) of 1094, 1177, and 698 S cm^{-1} for doping levels of 5, 10, and 50 mM, respectively.

Historically, doping level and main chain chemistries have been systematically engineered to achieve metallic transport properties; however, here we have the first demonstration that side chain engineering and removal can be used to access both semiconducting (*i.e.,* thermally activated) and metallic (*i.e.,* thermally deactivated) transport regimes. We note that most other PEDOT systems (including PSS and Tos doped samples) are thermally activated, and seldomly obtain metallic transport even after significant doping and processing optimizations.[64],[65] Polyaniline (PANI) is similar, where most processes and doping levels yield thermally activated electrical conductivities, but the proper synthesis, processing, and doping can yield thermally deactivated electrical conductivities.[66],[67],[68] In both PEDOT and PANI, it is believed that these processing and doping optimizations can yield metallic transport because they create a macroscopic percolated pathway of more metallic and ordered islands in a more disordered and/or insulative matrix. This is most obvious in studies where electrically insulative PSS is isolated from electrically conductive PEDOT, but also, this paradigm is akin to what we demonstrated herein; hydrolyzing and removing the electrically insulative side chains results in marked changes in charge transport by decreasing localization.

Conclusion

In summary, we report a fully solution-processable PEDOT bearing cleavable ester-based side chains. Following film formation and oxidative doping, this material has moderate σ (~65 S cm^{-1} with thermal annealing), the highest of any hydrocarbon functionalized PEDOT, and demonstrates semiconducting transport properties. Upon hydrolysis, the ester polymer films are converted to solvent resistant films of PEDOT(OH) with an increased density of electroactive material. These films, following comparable doping procedures to the parent ester polymer, demonstrate higher σ values (~700 S/cm) and metallic charge transport properties. Optimizing the doping of PEDOT(OH) leads to σ values averaging 1100-1200 S cm^{-1}, depending on the dopant used, with increasing film conductivity showing increased metallic behavior. These values are comparable to those for ethylene glycol/acid treated PEDOT:PSS[19],[25] or optimized camphor sulfonic acid (CSA) doped PANI.[67]

The σ reported here are the highest of any material prepared via direct arylation. Furthermore, PEDOT(OH) is the first material prepared via this route to show metallic transport, demonstrating the further potential of this synthetic route. Interestingly, unlike the initial materials studied using this methodology,[39] PEDOT(OH) films prepared via this method cannot be fully de-doped and rendered non-conductive using conventional methods (*i.e.,* chemical or electrochemical de-doping). It is currently believed this is a result of the exceptionally low onset of oxidation for these films.

The broad use of PEDOT(OH) for applications ranging from charge storage to neural electrodes make the improved processing and properties presented here of great interest for further investigation. In contrast to PEDOT:PSS, these doped PEDOT(OH) films are solvent resistant, while remaining hydrophilic, and not acidic. Additionally, most highly conductive PEDOT:PSS and PBTTT films are thin (20-60 nm thick), resulting in large sheet resistances despite the high σ values, as shown in Table S3. Perhaps the most comparable systems to this report are solution polymerized/processed PEDOT:Tos and PEDOT(OH):Tos, which are prepared on substrates by spin coating the monomers, oxidant, additives, and solvent onto a substate.[9] While PEDOT(OH):Tos prepared via this method can yield an σ of ~900 S cm^{-1}, spin coating limits control of film thickness and results in higher sheet resistance (see Table S3). In contrast, doped

PEDOT(OH) films prepared as reported here demonstrate high σ (> 1000 S cm^{-1}) in thick films (tested up to ~1 μm thick after cleavage), allowing for greater control of device operation and access to low sheet resistance films. Further tests are underway to apply this material in various applications and to probe the further potential of side chain cleavage to access metallic-like, highly conductive materials.

SUPPORTING INFORMATION

Monomer and polymer synthesis, processing and hydrolysis conditions, and instrumentation details, along with additional schemes, figures, and tables, can be found in the Supporting Information. Supporting information is available from the Wiley Online Library or from the author.

Data Availability Statement

The data that support the findings of this study are available from the corresponding author upon reasonable request.

AUTHOR INFORMATION

Corresponding Author

*E-mail jponder7@gatech.edu

Authors' Contributions

JFP designed the project, synthesized the materials, prepared/processed films for measurements, and performed various measurements (NMR, GPC, UV-vis-NIR, stylist profilometry, CV/DPV, etc.). SAG performed thermoelectric (including temperature-dependent) measurements and optical profilometry. AA performed XPS analysis and data interpretation, along with GIWAXS analysis. AAA performed electrochemical (CV, DPV, and spectroelectrochemistry) and thermal (TGA and DSC) measurements. JMR performed optical profilometry and ambient doping experiments. GF performed GIWAXS measurements. GMS assisted in acquiring GIWAXS user time and assisted

in the interpretation and contextualization of the GIWAXS data. JRR and SKY provided insight to the project and writing on the manuscript. The paper was written by JFP with the participation/input and approval of all the coauthors.

ORCID

James F. Ponder Jr.: 0000-0001-8093-1849

Shawn A. Gregory: 0000-0002-1027-0675

Amalie Atassi: 0000-0003-3218-680X

Abigail A. Advincula: 0000-0003-2210-7178

Joshua M. Rinehart: 0000-0001-8111-2749

Guillaume Freychet: 0000-0001-8406-798X

Gregory M. Su: 0000-0001-7495-8041

Shannon K. Yee: 0000-0002-1119-9938

John R. Reynolds: 0000-0002-7417-4869

CONFLICTS OF INTEREST

The authors declare no competing financial interest.

ACKNOWLEDGEMENTS

The authors thank BASF for providing 3,4-dimethoxythiophene. JFP, SAG, SKY, and JRR appreciate support from the Office of Naval Research (award numbers N00014-19-1-2162, N00014-20-1-2129, and N00014-22-1-2185). JFP thanks Walter P. Parker Jr. for assisting with contact angle measurements. AA appreciates the support of the National Science Foundation Graduate Research Fellowship under Grant No. DGE-1650044. AAA was supported by the Department of Defense (DoD) through the National Defense Science & Engineering Graduate Fellowship (NDSEG) Program.

TGA, DSC, and GPC measurements were performed at the Organic Materials Characterization Laboratory (OMCL) at Georgia Tech. Part of this work (XPS Analysis) was performed at the Georgia Tech Institute for Electronics and Nanotechnology, a member of the National Nanotechnology Coordinated Infrastructure, which is supported by the National Science

Foundation (Grant ECCS-1542174). Part of this work (GIWAXS) was performed at the beamline 12-ID of the National Synchrotron Light Source II, a U.S. Department of Energy (DOE) Office of Science User Facility operated for the DOE Office of Science by Brookhaven National Laboratory under Contract No. DE-SC0012704. The authors thank Dr. Madeleine P. Gordon for assistance in GIWAXS sample preparation and Dr. Mikhail Zhernenkov (NSLS-II) for assistance at the beamline.

REFERENCES

[1] F. Jonas, G. Heywang, W. Schmidtberg, Bayer AG, **1988**, DE 38 14 730 A1 (Bayer AG). Prior: April, 30.
[2] G. Heywang, F. Jonas, *Adv. Mater.* **1992**, *4*, 116-118.
[3] S. K. An. Elschner, W. Lövenich, U. Merker, K. Reuter, *PEDOT: Principles and Applications of an Intrinsically Conducting Polymer*, CRC Press, Boca Raton, FL, USA, **2011**.
[4] L. Groenendaal, F. Jonas, D. Freitag, H. Pielartzik, J. R. Reynolds, *Adv. Mater.* **2000**, *12*, 481-494.
[5] Y. Jiang, T. Liu, Y. Zhou, *Adv. Funct. Mater.* **2020**, *30*, 2006213.
[6] S. Maity, S. Datta, M. Mishra, S. Banerjee, S. Das, K. Chatterjee, *Polym. Adv. Technol.* **2021**, *32*, 1409-1427.
[7] Z. Rahimzadeh, S. M. Naghib, Y. Zare, K. Y. Rhee, *J. Mater. Sci.* **2020**, *55*, 7575-7611.
[8] D. M. De Leeuw, P. Kraakman, P. Bongaerts, C. Mutsaers, D. Klaassen, *Synth. Met.* **1994**, *66*, 263-273.
[9] Y. H. Ha, N. Nikolov, S. K. Pollack, J. Mastrangelo, B. D. Martin, R. Shashidhar, *Adv. Funct. Mater.* **2004**, *14*, 615-622.
[10] M. C. Morvant, J. R. Reynolds, *Synth. Met.* **1998**, *92*, 57-61.
[11] G. A. Sotzing, J. R. Reynolds, P. J. Steel, *Adv. Mater.* **1997**, *9*, 795-798.
[12] E. Poverenov, M. Li, A. Bitler, M. Bendikov, *Chem. Mater.* **2010**, *22*, 4019-4025.
[13] R. Singh, A. Kumar, *Org. Electron.* **2016**, *30*, 67-75.
[14] A. Kumar, J. R. Reynolds, *Macromolecules* **1996**, *29*, 7629-7630.
[15] H. Zhao, C.-Y. Liu, S.-C. Luo, B. Zhu, T.-H. Wang, H.-F. Hsu, H.-h. Yu, *Macromolecules* **2012**, *45*, 7783-7790.
[16] S. E. Atanasov, M. D. Losego, B. Gong, E. Sachet, J.-P. Maria, P. S. Williams, G. N. Parsons, *Chem. Mater.* **2014**, *26*, 3471-3478.
[17] M. Heydari Gharahcheshmeh, M. T. Robinson, E. F. Gleason, K. K. Gleason, *Adv. Funct. Mater.* **2021**, *31*, 2008712.
[18] L. V. Kayser, D. J. Lipomi, *Adv. Mater.* **2019**, *31*, 1806133.
[19] M. De Keersmaecker, A. W. Lang, A. M. Österholm, J. R. Reynolds, *ACS Appl. Mater. Interfaces* **2018**, *10*, 31568-31579.
[20] J. Wan, Y. Xia, J. Fang, Z. Zhang, B. Xu, J. Wang, L. Ai, W. Song, K. N. Hui, X. Fan, Y. Li, *Nano-Micro Letters* **2021**, *13*, 44.
[21] L. Manjakkal, A. Pullanchiyodan, N. Yogeswaran, E. S. Hosseini, R. Dahiya, *Adv. Mater.* **2020**, *32*, 1907254.

[22] W. Han, G. Ren, J. Liu, Z. Li, H. Bao, C. Liu, W. Guo, *ACS Appl. Mater. Interfaces* **2020**, *12*, 49297-49322.
[23] C.-Y. Lo, Y. Wu, E. Awuyah, D. Meli, D. M. Nguyen, R. Wu, B. Xu, J. Strzalka, J. Rivnay, D. C. Martin, L. V. Kayser, *Polym. Chem.* **2022**, 13, 2764-2775.
[24] J. Ouyang, *ACS Appl. Mater. Interfaces* **2013**, *5*, 13082-13088.
[25] H. Shi, C. Liu, Q. Jiang, J. Xu, *Adv. Electron. Mater.* **2015**, *1*, 1500017.
[26] J. Cameron, P. J. Skabara, *Mater. Horiz.* **2020**, *7*, 1759-1772.
[27] S. Akoudad, J. Roncali, *Electrochem. Commun.* **2000**, *2*, 72-76.
[28] E.-C. Cho, C.-W. Chang-Jian, B.-C. Ho, C.-C. Yu, Y.-S. Hsiao, K.-C. Lee, J.-H. Huang, *Dyes Pigm.* **2017**, *145*, 95-102.
[29] G. Nikiforidis, S. Wustoni, D. Ohayon, V. Druet, S. Inal, *ACS Appl. Energy Mater.* **2020**, *3*, 7896-7907.
[30] Y. Xiao, X. Cui, J. M. Hancock, M. Bouguettaya, J. R. Reynolds, D. C. Martin, *Sensors and Actuators B: Chemical* **2004**, *99*, 437-443.
[31] S. Y. Severt, N. A. Ostrovsky-Snider, J. M. Leger, A. R. Murphy, *ACS Appl. Mater. Interfaces* **2015**, *7*, 25281-25288.
[32] A. Zhuang, Y. Bian, J. Zhou, S. Fan, H. Shao, X. Hu, B. Zhu, Y. Zhang, *ACS Appl. Mater. Interfaces* **2018**, *10*, 35547-35556.
[33] Y.-S. Hsiao, Y.-H. Liao, H.-L. Chen, P. Chen, F.-C. Chen, *ACS Appl. Mater. Interfaces* **2016**, *8*, 9275-9284.
[34] T.-Y. Kim, S. Lee, D. Jeong, T. K. Lee, B. S. Kim, I. S. Chae, Y. S. Kang, *ACS Appl. Energy Mater.* **2018**, *1*, 290-295.
[35] H. Dong, E. Zheng, Z. Niu, X. Zhang, Y.-Y. Lin, P. Jain, Q. Yu, *ACS Appl. Mater. Interfaces* **2020**, *12*, 17571-17582.
[36] C. Edder, P. B. Armstrong, K. B. Prado, J. M. J. Frechet, *ChemComm* **2006**, 1965-1967.
[37] Z. C. Smith, D. M. Meyer, M. G. Simon, C. Staii, D. Shukla, S. W. Thomas, *Macromolecules* **2015**, *48*, 959-966.
[38] B. D. Reeves, E. Unur, N. Ananthakrishnan, J. R. Reynolds, *Macromolecules* **2007**, *40*, 5344-5352.
[39] J. F. Ponder, S. A. Gregory, A. Atassi, A. K. Menon, A. W. Lang, L. R. Savagian, J. R. Reynolds, S. K. Yee, *J. Am. Chem. Soc.* **2022**, *144*, 1351–1360.
[40] L. A. Estrada, J. J. Deininger, G. D. Kamenov, J. R. Reynolds, *ACS Macro Letters* **2013**, *2*, 869-873.
[41] A. L. Jones, M. De Keersmaecker, I. Pelse, J. R. Reynolds, *Macromolecules* **2020**, *53*, 7253-7262.
[42] A. Lenz, H. Kariis, A. Pohl, P. Persson, L. Ojamäe, *Chem. Phys.* **2011**, *384*, 44-51.
[43] T. Prosa, M. Winokur, J. Moulton, P. Smith, A. Heeger, *Macromolecules* **1992**, *25*, 4364-4372.
[44] D. Kim, I. Zozoulenko, *J. Phys. Chem. B* **2019**, *123*, 5160-5167.
[45] J. F. Ponder Jr., A. K. Menon, R. R. Dasari, S. L. Pittelli, K. J. Thorley, S. K. Yee, S. R. Marder, J. R. Reynolds, *Adv. Energy Mater.* **2019**, *9*, 1900395.
[46] S. A. Gregory, J. F. Ponder, S. L. Pittelli, M. D. Losego, J. R. Reynolds, S. K. Yee, *ACS Appl. Polym. Mater.* **2021**, *3*, 2316-2324.
[47] J. F. Ponder, A. M. Österholm, J. R. Reynolds, *Macromolecules* **2016**, *49*, 2106-2111.
[48] J. F. Ponder, A. M. Österholm, J. R. Reynolds, *Chem. Mater.* **2017**, *29*, 4385-4392.

[49] A. A. Advincula, A. L. Jones, K. J. Thorley, A. M. Österholm, J. F. Ponder, J. R. Reynolds, *Chem. Mater.* **2022**, *34*, 4633-4645.
[50] N. G. Connelly, W. E. Geiger, *Chem. Rev.* **1996**, *96*, 877-910.
[51] B. X. Dong, C. Nowak, J. W. Onorato, T. Ma, J. Niklas, O. G. Poluektov, G. Grocke, M. F. DiTusa, F. A. Escobedo, C. K. Luscombe, P. F. Nealey, S. N. Patel, *Chem. Mater.* **2021**, *33*, 741-753.
[52] J. Heinze, B. A. Frontana-Uribe, S. Ludwigs, *Chemical Reviews* **2010**, *110*, 4724-4771.
[53] A. M. Österholm, J. F. Ponder, M. De Keersmaecker, D. E. Shen, J. R. Reynolds, *Chem. Mater.* **2019**, *31*, 2971-2982.
[54] I. Salzmann, G. Heimel, M. Oehzelt, S. Winkler, N. Koch, *Acc. Chem. Res.* **2016**, *49*, 370-378.
[55] I. Zozoulenko, A. Singh, S. K. Singh, V. Gueskine, X. Crispin, M. Berggren, *ACS Appl. Polym. Mater.* **2019**, *1*, 83-94.
[56] R. M. Pankow, L. Ye, N. S. Gobalasingham, N. Salami, S. Samal, B. C. Thompson, *Polym. Chem.* **2018**, *9*, 3885-3892.
[57] S. A. Gregory, A. K. Menon, S. Ye, D. S. Seferos, J. R. Reynolds, S. K. Yee, *Adv. Energy Mater.* **2018**, *8*, 1802419.
[58] I. E. Jacobs, Y. Lin, Y. Huang, X. Ren, D. Simatos, C. Chen, D. Tjhe, M. Statz, L. Lai, P. A. Finn, W. G. Neal, G. D'Avino, V. Lemaur, S. Fratini, D. Beljonne, J. Strzalka, C. B. Nielsen, S. Barlow, S. R. Marder, I. McCulloch, H. Sirringhaus, *Adv. Mater.* **2022**, *34*, 2102988.
[59] S. Rudd, J. F. Franco-Gonzalez, S. Kumar Singh, Z. Ullah Khan, X. Crispin, J. W. Andreasen, I. Zozoulenko, D. Evans, *J Polym Sci B Polym Phys* **2018**, *56*, 97-104.
[60] Z. U. Khan, O. Bubnova, M. J. Jafari, R. Brooke, X. Liu, R. Gabrielsson, T. Ederth, D. R. Evans, J. W. Andreasen, M. Fahlman, X. Crispin, *J. Mater. Chem. C* **2015**, *3*, 10616-10623.
[61] Z. Peng, L. Ye, H. Ade, *Mater. Horiz.* **2022**.
[62] I. E. Jacobs, G. D'Avino, V. Lemaur, Y. Lin, Y. Huang, C. Chen, T. F. Harrelson, W. Wood, L. J. Spalek, T. Mustafa, *J. Am. Chem. Soc.* **2022**, *144*, 3005-3019.
[63] S. A. Gregory, Hanus, Riley, Atassi, Amalie, Rinehart, Joshua M., Wooding, Jamie P., Menon, Akanksha K., Losego, Mark D., Snyder, G. Jeffery, Yee, Shannon K. , *Nat. Mater.* **2021**, 20, 1414-1421.
[64] A. C. Hinckley, S. C. Andrews, M. T. Dunham, A. Sood, M. T. Barako, S. Schneider, M. F. Toney, K. E. Goodson, Z. Bao, *Adv. Electron. Mater.* **2021**, *7*, 2001190.
[65] W. Shi, Q. Yao, S. Qu, H. Chen, T. Zhang, L. Chen, *NPG Asia Materials* **2017**, *9*, e405-e405.
[66] C. Yoon, M. Reghu, D. Moses, Y. Cao, A. Heeger, *Synth. Met.* **1995**, *69*, 273-274.
[67] K. Lee, S. Cho, S. Heum Park, A. J. Heeger, C.-W. Lee, S.-H. Lee, *Nature* **2006**, *441*, 65-68.
[68] C. Yoon, M. Reghu, D. Moses, A. Heeger, Y. Cao, *Synth. Met.* **1994**, *63*, 47-52.

ToC Figure:

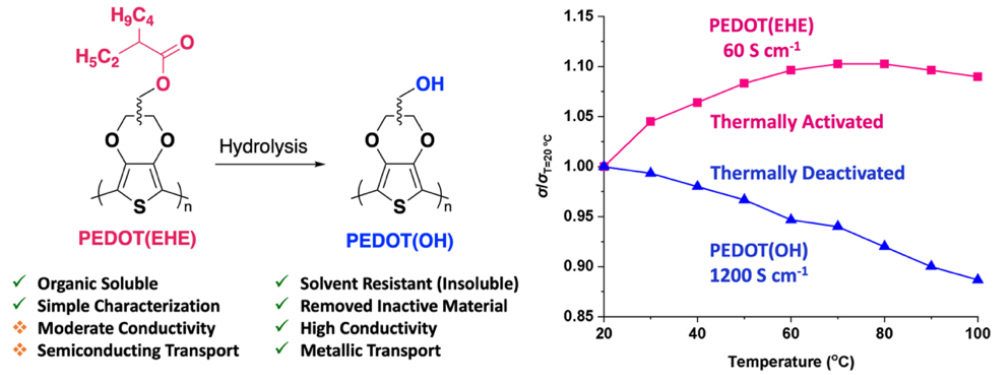

ToC Text: Functionalization of poly(3,4-ethylenedioxythiophene) (PEDOT) with ester-based side chains allow for solution processing and moderate electrical conductivity. Hydrolysis of these side chains leaves hydroxymethyl functional groups on the polymer, increases the relative amount of electroactive material, significantly increases electrical conductivity to greater than 1,000 S cm^{-1}, and changes the transport mechanism from hopping-like to metallic.